Growth and Optical Properties of Faceted Hexagonal ZnO Nanotubes

Yanhong Tong,[†,‡,§] Yichun Liu,[*,†] Changlu Shao,[†] Yuxue Liu,[†] Changshan Xu,[†] Jiying Zhang,[‡] Youming Lu,[‡] Dezhen Shen,[‡] and Xiwu Fan[‡]

Center for Advanced Opto-Electronic Functional Material Research, Northeast Normal University, Changchun 130024, People's Republic of China, Key Laboratory of Excited-State Process, Changchun Institute of Optics, Fine Mechanics and Physics, Chinese Academy of Sciences, Changchun 130033, People's Republic of China, and Graduate School of Chinese Academy of Sciences, Beijing 100039, People's Republic of China

Received: November 17, 2005; In Final Form: March 6, 2006

Well-faceted hexagonal ZnO nanotubes were synthesized by a simple hydrothermal method and the subsequent aging process without any catalysts or templates. The formation of the tubular structure is closely linked to the polarity of ZnO and the selective adsorption behavior of Zn^{2+} amino complexes. The surface-related optical properties were studied with use of Raman and photoluminescence spectra. It was found that the oxygen vacancy-related visible emission intensity decreased while surface defect-related visible emission intensity increased when the nanotubes were annealed in oxygen ambient. The anomalous enhancement of PL integrated intensity with the temperature shows fairly high surface state density existing in ZnO nanotubes.

Introduction

Recently, one-dimensional (1D) ZnO nanostructures, especially ZnO nanowires, nanorods, and nanobelts, have been extensively studied due to their potential applications in nanoscale electronic and optoelectronic devices.[1−3] In contrast, few publications on the preparation of ZnO nanotubes have been reported because the tubular form is generally limited in layered materials such as carbon nanotube so that it seems hard to obtain the tubular structure for the nonlayered ZnO material. It is widely acknowledged that the special hollow structure provides 1D ZnO with more prominent advantages than other 1D ZnO materials. For example, the formation of tubes facilitates enhancing the confinement effect in 1D structures and tuning the electronic properties of materials in a wider range.[4,5] Moreover, a larger surface area−volume ratio in tubular structure provides an effective way to optimize the performances of various devices including dye-sensitized photovoltaic cells, catalysts, gas sensors, and hydrogen storage.[6,7]

ZnO nanotubes have only been fabricated by vapor phase deposition,[8] thermal oxidation,[9] a template-assisted method, and a hydrothermal process.[10,11] Almost all reports about ZnO nanotubes are focused on morphologies, synthetic methods, and growth mechanisms. As mentioned above, however, the increased surface area is a key feature for tubular ZnO. Inevitably, fairly high surface state density will significantly modify or alter the chemical and physical properties of materials, which can be reflected in Raman and photoluminescence (PL) spectra. As we know, the inelastic scattering of light from the crystal lattice vibrations produces Raman spectra. Obviously, surface properties, such as surface area, surface bonding, and surface adsorption, will affect crystal structure and vibration modes, and hence alter the characteristic Raman frequency from its ideal value (corresponding to high quality material). When the energy of the excitation light is higher than the band gap, the excitation light is mainly absorbed at the near-surface region.[12] This indicates that the surfaces play a significant role in the process of the luminescence and the surface states will have profound effects on the luminescence properties. Therefore, further studying the surface features of ZnO nanostructures by Raman scattering and PL techniques and a deeper understanding of the impact of surfaces on the nanostructures are obviously urged in order to flexibly control and design their surface behavior.

Here, we present a novel chemical route to prepare ZnO nanotubes by a hydrothermal technique and a subsequent aging process. The reaction temperature is below 100 °C. The growth mechanism of ZnO nanotubes is studied in detail, and the influence of unique surface features on the optical properties is also investigated.

Experimental Section

All chemicals are analytical grade reagents and were purchased from Beijing Chemical Company.

ZnO nanotubes were fabricated by the following procedure. Zinc nitrate (5 mL of 0.05 mol/L) and methenamine aqueous (5 mL of 0.05 mol/L) solutions were respectively added into a Teflon-lined autoclave with a capacity of 15 mL. Subsequently, sealed and heated at 90 °C for 3 h, the autoclave was cooled to room temperature. After the supernatant was removed, the remnants were transferred into a 10 mL open glass bottle and shelved in air at 60 °C for days and the white powder was obtained.

The morphology of the powder was characterized by a scanning electron microscope (SEM; Hitachi S-4300). The Raman spectrum was measured by using an Ar^+ laser at 488 nm and recorded in the backscattering geometry. The PL spectra were measured by using an excitation wavelength of 325 nm with a power of 50 mW. All the optical measurements were performed on a LABRAM-UV Raman microspectrometer (Jobin Yvon).

* Author to whom correspondence should be addressed. E-mail: ycliu@nenu.edu.cn. Phone: +86-431-5099168. Fax: +86-431-5684009.
† Center for Advanced Opto-Electronic Functional Material Research.
‡ Key Laboratory of Excited-State Process.
§ Graduate School of Chinese Academy of Sciences.

10.1021/jp056654h CCC: $33.50
Published on Web 07/13/2006

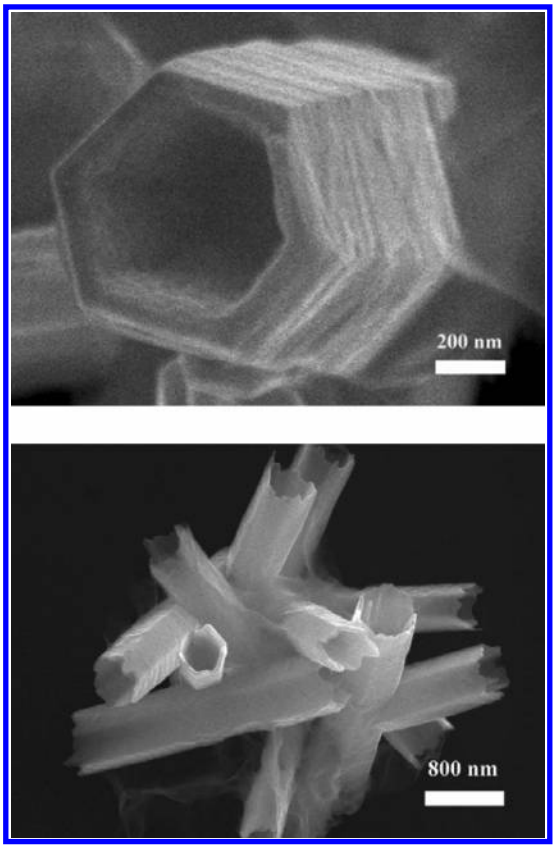

Figure 1. SEM images of ZnO nanotubes synthesized in two steps.

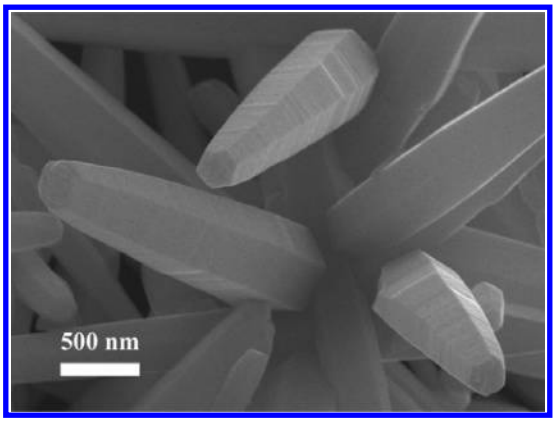

Figure 2. SEM image of ZnO nanotowers via the first-step hydrothermal process.

Results and Discussion

Figure 1 shows the SEM images of ZnO nanotubes. The high-magnification image reveals that the single tube is a hollow structure with rough surfaces, which indicates a layer-stack structure. The length of ZnO nanotubes is in the range of 1−3 μm and the wall thickness is 50−100 nm, respectively. The cross section is hexagonally faceted, providing strong evidence that the single nanotube grows along the *c*-axis direction. The ZnO nanotubes have a hexagonal wurtzite structure confirmed by the XRD result (not shown here).

To investigate the growth mechanism of the hollow structure, the product without the second step aging process was centrifugated and washed with deionized water to keep the exact morphology of the as-formed crystal after the first-step hydrothermal reaction. As shown in Figure 2, it is only the solid ZnO nanotowers that were formed during the hydrothermal process. This implies that tubular ZnO was produced through the second

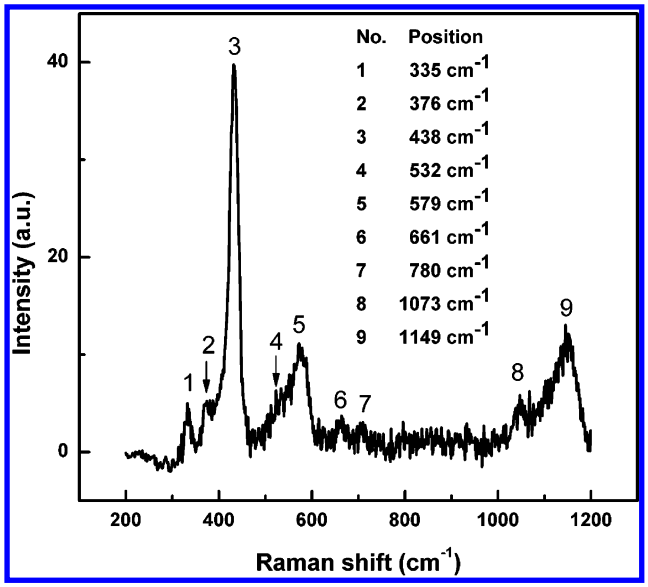

Figure 3. Raman spectrum of ZnO nanotubes.

step aging process. The whole growth process can be assumed to be related to the polarity of ZnO and the adsorption effect of Zn^{2+} amino complexes. ZnO is composed of nonpolar $\{01\bar{1}0\}$ and polar {0001} faces. The nonpolar faces have lower surface energy while the polar faces have relatively higher surface energy. In the growth process, crystal tends to minimize the total surface energy by growing along the [0001] direction. The growth rate is relatively high because of the high supersaturation degree at the early stage. A fast growth makes the atomic steps exist on the side surfaces.[13] As a result, the 1D tower-like structure was formed at the first step process. On the other hand, ammonium salts tend to bind with Zn^{2+} ions generating Zn^{2+} amino complexes. They primarily adsorb on the six prismatic side planes slowing down the growth velocity of the side surfaces.[13] This also facilitates the growth of the 1D structure. After the growth of ZnO nanotowers reaches a certain equilibrium at the second step process, the rate of dissolution is faster than the rate of formation (Ostwald ripening). At this case, the polar surfaces having the higher energy will be dissolved in priority to decrease the system energy in the subsequent aging process. The formed inner walls in the process of dissolution have the same feature as the outer walls, i.e., adsorbing the Zn^{2+} amino complexes and slowing down the dissolving velocity of side faces. Therefore, the tubular structure is formed in the second step aging process. It is worth noting that the roughness of ZnO nanotubes is much larger than that of ZnO nanotowers, indicating that the multilayer side surfaces also originate from the dissolution of ZnO nanotowers.

Zn^{2+} amino complexes play an important role in the whole process. However, it is not absolutely necessary for the formation of the 1D solid ZnO structure but determinative for the formation of hollow structure. Peterson et al. have obtained 1D ZnO nanocolumns from NaOH solution without adding any ammonia or ammonium salts.[14] With the aging process, however, the length and width of the ZnO nanocolumns are simultaneously dissolved and no tubular structures were obtained. These results indicate that Zn^{2+} amino complexes only modify or facilitate the formation of the 1D solid ZnO nanostructure; however, these complexes play an indispensable role in the process of forming the tubular ZnO nanostructure. Additionally, the polarity of ZnO is a necessary factor for the 1D solid and hollow structure in the whole growth process according to the growth mechanism of ZnO nanotubes mentioned above.

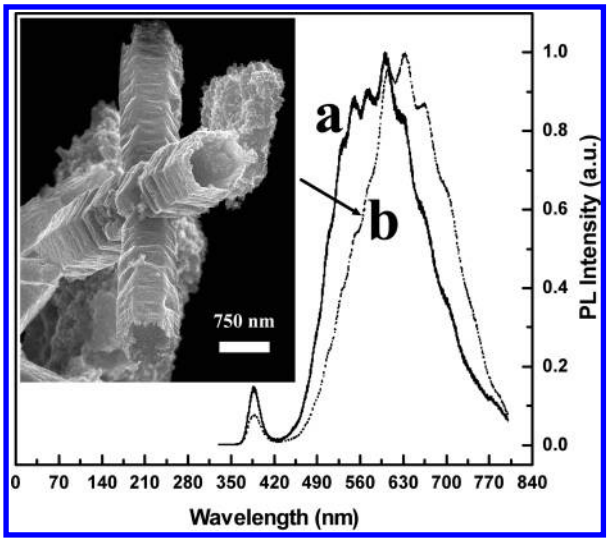

Figure 4. Room temperature photoluminescence spectra of ZnO nanotubes: (a) without annealing and (b) annealed for 30 min at 400 °C in oxygen ambient. The inset is the SEM image of annealed ZnO nanotubes.

Figure 3 illustrates the background-subtracted Raman spectrum of the ZnO nanotubes. ZnO is a wurtzite crystal with C_{6v}^4 symmetry, which is one of the simplest uniaxial crystals. For the perfect infinite ZnO crystal, in first-order Raman scattering, only the optical phonons at the center of the Brillouin zone are involved. In group theory, $\Gamma\text{opt} = A_1(z) + 2B_1 + E_1(x,y) + 2E_2$, where x, y, and z in parentheses represent the polarization directions. A_1 and E_1 modes are polar and therefore split into transverse and longitudinal optical (TO and LO) components. The two are both Raman active and infrared active. The E_2 modes are Raman active only and the B_1 modes are infrared and Raman inactive (silent modes). In addition, in an ideal backscattering configuration, A_1(TO), A_1(LO), E_1(TO), and E_2 modes are allowed in first-order Raman scattering when the incidence direction with respect to the crystal axis is not defined.[15] Although each ZnO nanotube is *c*-axis oriented, the whole nanotubes are randomly arrayed. Therefore, the three aforementioned modes, i.e., A_1(TO) at 376 cm^{-1}, A_1(LO) at 532 cm^{-1}, and E_2(high) at 438 cm^{-1},[16] appear in this geometry, as shown in Figure 3. However, E_1(TO) at 407 cm^{-1} cannot be observed.[17] A possible explanation is as follows. As the characteristic peak of hexagonal wurtzite ZnO, the E_2(high) at 438 cm^{-1} is very intense and has a full width at half-maximum (fwhm) of 21 cm^{-1}. The asymmetrical and line-broadening characteristics mask E_1(TO) on left-hand side of E_2(high). Obviously, the peak at 532 cm^{-1} is broadened, which indicates that it may be a compound mode mixed with A_1(LO) and surface modes.[18] The peak at 579 cm^{-1} is attributed to the E_1(LO) mode.[16] This mode is not allowed in the backscattering configuration. Its appearance may be due to the q-selection rule relaxation.[19] According to the SEM results, the large surface area, high surface roughness, and layer−layer structure imply the pronounced enhancement of surface activity compared with that of bulk crystal. This may activate the normally forbidden E_1(LO) mode. In addition, the peaks at 335, 661, 780, 1073, and 1149 cm^{-1} are due to multiple phonon scattering processes.[16] In Raman measurement, a large luminescence background can be observed through the whole Raman spectrum, which corresponds to the green wavelength region from 492 to 519 nm. A green emission band has been observed in the PL spectrum of ZnO by the above-band gap excitation and its luminescence mechanism has been extensively investigated.

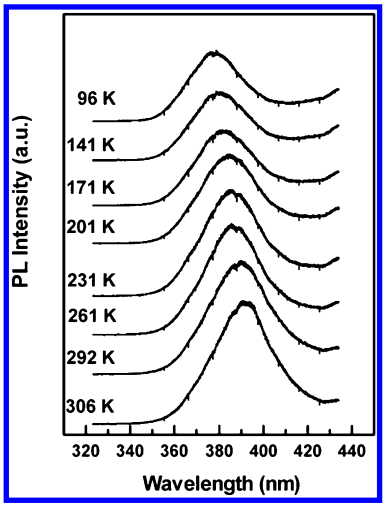

Figure 5. Dependence of the photoluminescence spectra of ZnO nanotubes on the temperature from 96 to 306 K.

Vanheusden et al. assigned the green emission to the recombination of electrons in singlely occupied oxygen vacancies with photoexcited holes in the valence band.[20] Dijken et al. proposed that the emission originated from the recombination between a deeply trapped hole in a V_O^{**} center and a shallowly trapped electron.[21] Now, the nature of the green emission still remains controversial. However, it is widely accepted that oxygen vancancies are responsible for the green emission. On the other hand, there are a large number of intrinsic defects existing in ZnO. In particular, for tubular ZnO nanostructures, abundant surface defects will lead the distribution of surface energy levels forming the surface energy band. The sub-bandgap excitation at 488 nm can induce the excitation of surface states. Therefore, the green emission in Raman measurement may be related to surface states.

Figure 4a is the room temperature PL spectrum of ZnO nanotubes. For comparison, the PL spectrum of ZnO nanotubes annealed for 30 min at 400 °C in oxygen ambient is also shown in Figure 4. The inset is the SEM image of annealed nanotubes. Every PL spectrum possesses a common feature that consists of an ultraviolet (UV) PL peak and a visible emission band. Generally, the UV peak is due to the exciton recombination while the visible emission centered at about 560 nm ranging from 440 to 600 nm is associated with oxygen vacancies. In the current PL measurements, the visible emission of ZnO nanotubes has a much broader band from 440 to 800 nm, which can only be observed in ZnO nanostructures in other literature.[22] Considering the large surface area−volume ratio in nanostructures, the broadening of the visible emission can be ascribed to abundant surface defects. A large quantity of defects and impurities at the surface of ZnO nanotubes can provide new states which can contribute as visible luminescence centers and broaden the visible emission band. The annealing treatment of the nanotubes in oxygen ambient further confirms this point. When ZnO nanotubes are annealed in oxygen ambient, the number of oxygen vacancies in ZnO nanotubes will decrease under oxygen-rich condition. On the other hand, the SEM image in the inset of Figure 4 shows that the annealed ZnO nanotubes have a larger surface roughness, indicating the existence of more surface defects. As a result, the oxygen vacancy-related visible emission intensity decreases while surface defect-related visible emission intensity increases, leading to the visible emission center position shifting from 560 to 630 nm, as shown in Figure 4.

Figure 5 shows UV PL spectra of the ZnO nanotubes for different temperatures in the range from 96 to 306 K. An

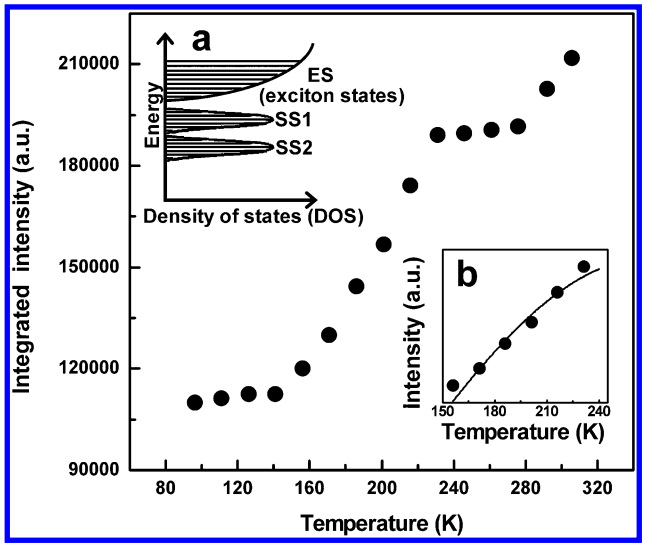

Figure 6. Experimental temperature dependence of ultraviolet photoluminescence integrated intensity ranging from 96 to 306 K for ZnO nanotubes. Inset: (a) schematic diagram of energy against exciton state density and localized-state density and (b) temperature dependence of the luminescence intensity ranging from 156 to 231 K. The solid curve represents a theoretical fitting result.

anomalous feature can be found that the emission intensity increases with the increasing temperature. The temperature dependence of the luminescence integrated intensity is clearly shown in Figure 6 by closed circles. Generally, the PL intensity decreases with an increase of temperature and the temperature dependence satisfies the Arrhenius behavior as a consequence of temperature quenching effects. The anomalous enhancement of PL intensity with the temperature can be caused by spatially localized excitons at surface states and can be explained by the relative change in carrier populations with temperatures.[23] As mentioned above, the luminescence process is quite complicated. Raman and room temperature PL spectra have clearly indicated the existence of abundant surface states in ZnO nanotubes which can trap photogenerated carriers. An increase in temperature makes more trapped carriers obtain enough thermal energy to escape from the surface states. As a result, an increase in the number of free carriers leads to an increase in the combination probability of electrons and holes, and hence makes the UV PL intensity increase with the increase of temperature. Further, it is observed that the UV PL intensity remains increasing up to the limit of detection at 306 K, indicating that our obtained ZnO nanotubes possess high localized state density. The plot of the PL intensity as a function of temperature has two plateaus in the range of 96−141 and 231−276 K, which can be related to two different localized states, as shown in the inset of Figure 6. The inset in upper left corner of Figure 6 is the schematic diagram of energy against exciton state density and localized state density. From Figure 6, the intensity shows only a weak increase when the temperature increases from 96 to 141 K, suggesting that the temperature is not high enough to activate a number of trapped carriers and the number of the carriers thermally escaping from the surface states is almost equivalent to those excitons which are thermalized with the lattice by emitting phonons at low temperature. With the increase of the temperature from 156 to 231 K, the carriers trapped at shallower surface states (SS1), which have a smaller active energy, can gradually escape from shallow traps and contribute to exciton emission. In this case, the corresponding thermally quenching effect is weak in comparison with the strong thermal ionization effect, resulting in a rapid increase of PL intensity. In the range of 156 to 231 K, the temperature dependence of the PL integrated intensity can be fitted by[24]

$$I(T) = \frac{I_0}{1 + \nu_0 \exp[(T/T_n) + (T_r/T)]}$$

where I_0 is the initial intensity, ν_0 is reduced frequency, T_n is the characterizitic nonradiative temperature reflecting a Berthelot-type behavior, and T_r is the characterizitic radiative temperature associated with a tunneling escape process and a thermally activated process.[25] The fitting plot is shown in the inset of Figure 6. We obtain $T_n = 378$ K and $T_r = 203$ K, respectively corresponding to 36 and 19 meV. The good agreement between the experimental data and the theoretical curve also confirms the disorder nature existing in the ZnO system.[24] When temperature continues to increase from 231 to 276 K, there are a few carriers left at SS1 and most of the trapped carriers at deeper surface states (SS2) do not have enough thermal energy to escape. Therefore, the total escape effect weakens, which makes the thermal ionization effect of excitons appreciable and the PL intensity present a weak increase. When temperature is over 276 K, abundant trapped carriers at SS2 begin to be activated and hence a more rapid increase of PL intensity occurs at elevated temperature. The anomalous temperature dependence of integrated intensity shows the surface state density in ZnO nanotubes is quite high so as to overrun the influence of temperature quenching and even alter the PL properties.

Conclusions

In summary, based on the formation of ZnO nanotowers in the first step, ZnO tubular structures can be obtained by the subsequent aging process. SEM images exhibit that ZnO nanotubes have a hexagonal cross section, rough surfaces, and multilayer structure. The formation of the tubular structure is closely linked to the polarity of ZnO and the selective adsorption effect of Zn^{2+} amino complexes. Accordingly, this synthesis route is also feasible for the fabrication of the tubular structures of other polar oxide materials. The Raman and PL spectra indicate high state density localized at the surface of ZnO nanotubes. The unique tubular nanostructure with rough surfaces and layer−layer structure can provide a direct path for electrical transport while simultaneously maintaining a large surface area, indicating promising applications as dye-sensitized photovoltaic cells, catalysts, gas sensors, and hydrogen storage devices.

Acknowledgment. This work is supported by the National Natural Science Foundation of China (Grant Nos. 60376009, 60278031 and 60576040), the Cultivation Fund of the Key Scientific and Technical Innovation Project, and Ministry of Education of China (Grant No. 704017).

References and Notes

(1) Huang, M. H.; Mao, S.; Feick, H.; Yan, H. Q.; Wu, Y. Y.; Kind, H.; Weber, E.; Russo, R.; Yang, P. D. *Science* **2001**, *292*, 1897.
(2) Park, W. I.; Kim, D. H.; Jung, S. W.; Yi, G. C. *Appl. Phys. Lett.* **2002**, *80*, 4232.
(3) Pan, Z. W.; Dai, Z. R.; Wang, Z. L. *Science* **2001**, *291*, 1947.
(4) Xing, Y. J.; Xi, Z. H.; Zhang, X. D.; Song, J. H.; Wang, R. M.; Xu, J.; Xue, Z. Q.; Yu, D. P. *Solid State Commun.* **2004**, *129*, 671.
(5) Bakkers, E. P. A. M.; Verheijen, M. A. *J. Am. Chem. Soc.* **2003**, *125*, 3440.
(6) Li, Q. H.; Gao, T.; Wang, Y. G.; Wang, T. H. *Appl. Phys. Lett.* **2005**, *86*, 123117.
(7) Wan, Q.; Lin, C. L.; Yu, X. B.; Wang, T. H. *Appl. Phys. Lett.* **2004**, *84*, 124.

(8) Jeong, J. S.; Lee, J. Y.; Cho, J. H.; Suh, H. J.; Lee, C. J. *Chem. Mater*. **2005**, *17*, 2752.

(9) Zhang, X. H.; Xie, S. Y.; Jiang, Z. Y.; Zhang, X.; Tian, Z. Q.; Xie, Z. X.; Huang, R. B.; Zheng, L. S. *J. Phys. Chem. B* **2003**, *107*, 10114.

(10) Wu, G. S.; Xie, T.; Yuan, X. Y.; Li, Y.; Yang, L.; Xiao, Y. H.; Zhang, L. D. *Solid State Commun.* **2005**, *134*, 485.

(11) Vayssieres,L.; Keis, K.; Hagfeldt, A.; Lindquist, S. *Chem. Mater*. **2001**, *13*, 4395.

(12) Skromme, B. J. In *Handbook of Compound Semiconductors*; Holloway, P. H., McGuire, G. E., Eds.; Noyes Publications: Park Ridge, NJ, 1995; p 689.

(13) Liu, B.; Zeng, H. C. *Langmuir* **2004**, *20*, 4196.

(14) Peterson, R. B.; Fields, C. L.; Gregg, B. A. *Langmuir* **2004**, *20*, 5114.

(15) Decremps, F.; Pellicer-Porres, J.; Saitta, A. M.; Chervin, J. C.; Polian, A. *Phys. Rev. B* **2002**, *65*, 092101.

(16) Wang, R. P.; Xu, G.; Jin, P. *Phys. Rev. B* **2004**, *69*, 113303.

(17) Damen, T. C.; Porto, S. P. S.; Tell, B. *Phys. Rev.* **1966**, *142*, 570.

(18) Tzolov, M.; Tzenov, N.; Dimova-Malinovska, D.; Kalitzova, M.; Pizzuto, C.; Vitali, G.; Zollo, G.; Ivanov, I. *Thin Solid Films* **2000**, *379*, 28.

(19) Katsikini, M.; Papagelis, K.; Paloura, E. C.; Ves, S. *J. Appl. Phys.* **2003**, *94*, 4389.

(20) Vanheusden, K.; Warren, W. L.; Seager, C. H.; Tallant, D. R.; Voigt, J. A.; Gnade, B. E. *J. Appl. Phys.* **1996**, *79*, 7983.

(21) van Dijken, A.; Meulenkamp, E. A.; Vanmaekelbergh, D.; Meijerink, A. *J. Phys. Chem. B* **2000**, *104*, 1715.

(22) Greene, L. E.; Law, M.; Goldberger, J.; Kim, F.; Johnson, J. C.; Zhang, Y. F.; Saykally, R. J.; Yang, P. D. *Angew. Chem., Int. Ed.* **2003**, *42*, 3031.

(23) Jiang, W. H.; Ye, X. L.; Xu, B.; Xu, H. Z.; Ding, D.; Liang, J. B.; Wang, Z. G. *J. Appl. Phys.* **2000**, *88*, 2529.

(24) John, G. C.; Singh, V. A. *Phys. Rev. B* **1996**, *54*, 4416.

(25) Suemoto, T.; Tanaka, K.; Nakajima, A. *Phys. Rev. B* **1994**, *49*, 11005.